Field distribution in polymeric MV-HVDC model cable under temperature gradient

Simulation and space charge measurements

Thi Thu Nga Vu[1,4], **Gilbert Teyssedre**[1,2], **Bertrand Vissouvanadin**[1], **Séverine Le Roy**[1,2], **Christian Laurent**[1,2], **Mohamed Mammeri**[3], **Isabelle Denizet**[3]

1. LAPLACE, Université de Toulouse ; UPS, INPT ; 118 route de Narbonne, 31062 Toulouse cedex 9, France

gilbert.teyssedre@laplace.univ-tlse.fr

2. LAPLACE ; CNRS, 31062 Toulouse, France

3. SilecCable, rue de Varennes Prolongée, 77876 Montereau Cedex

4. Electric University Power, 235 Hoang Quoc Viet Street, Hanoi, Vietnam

ABSTRACT. *One of the major problems regarding the development of HVDC cables is space charge build-up within the insulation of the cable which is nowadays mostly made with polymeric materials. The objective of this paper is to evaluate the influence of temperature gradient on space charge accumulation and electric field distribution in model medium voltage cables (MV-HVDC). These charge/field distributions are estimated by direct measurement or modelled from the temperature and field dependencies of material conductivity. Differences between model and measurement are discussed.*

RÉSUMÉ. *Un des problèmes rencontrés dans le développement de câbles HVDC est l'accumulation de charges dans les matériaux isolants, en particulier les isolants polymères, destinés à réaliser l'isolation de ces câbles. L'objectif de cette contribution est d'évaluer l'influence d'un gradient de température sur l'accumulation de charges et la distribution de champ électrique dans des câbles moyenne tension modèles (MV-HVDC). Ces distributions de charge/champ sont estimées par la mesure directe ou modélisées à partir de la dépendance en température et en champ de la conductivité mesurée expérimentalement. Les écarts entre modèle et mesure sont discutés.*

KEYWORDS: *HVDC power cables, space charge, electrical conductivity, stress inversion, crosslinked polyethylene, extruded insulation.*

MOTS-CLÉS : *câbles d'énergie HVDC, charge d'espace, conductivité électrique, inversion de contrainte, polyéthylène réticulé, isolation extrudée.*

DOI:10.3166/EJEE.17.307-325

1. Introduction

Unprecedented growth of energy transport projects through high voltage direct current – HVDC – links is found today all over the world which is related to the apparition of new converter technologies, the development of distributed energy sources and the need for network interconnections (Mazzanti *et al.,* 2011). One problem encountered in the development of HVDC cables (submarine links, landfilled links) is space charge accumulation in cable insulation.

When the amount of charges accumulated in the insulator is sufficiently high, local field may exceed the breakdown dielectric field of the material and thus cause failure. In addition, the current flowing in the conductor of the cable produces heat by Joule effect, resulting in a thermal gradient along the cable radius. If under HVAC stress, the capacitive-shaped field distribution is rather insensitive to such a thermal gradient, it is not the case in HVDC due to the resistive field distribution and the large temperature – and field – dependencies of the material electrical conductivity. The association of insulating materials of different nature, as in joints and cable terminations, coupled to these non-linear effects and to thermal gradients, makes it difficult the prediction of field distributions in service conditions. To partially overcome these difficulties, specific measurement techniques now provide access to charge density and field distributions in the bulk of the cable insulation, and are essential to more accurately design insulations.

Among the various possible mechanisms of charge accumulation, the one resulting from conductivity gradient, originating from the thermal gradient in the insulation is the most straightforward and has been the subject of many studies. Although the effects on field distributions have long been known, interest in space-charge approach actually starts with the work of McAllister *et al.* (1994) who investigated the charge accumulation phenomenon from a macroscopic point of view. In their work, charge accumulation is considered to be the consequence of a non-uniform electrical conductivity. The effects of temperature and electric field on conductivity were considered in this case. An expression of space charge distribution in steady state conditions in polymer insulated cable subject to a DC stress has been derived assuming conductivity increases exponentially with temperature and through a power function with electric field.

From the assumption on the temperature dependence of conductivity, using Maxwell's Equation, it can be shown that the electric field distribution in the cable insulation, in cylindrical geometry and under steady state condition is given by Fabiani *et al.* (2008):

$$E(r) = E_0 \frac{r_0 \sigma_0}{r \sigma(r)} \tag{1}$$

where E_0 and σ_0 are respectively the electric field and conductivity at the reference position r_0. Charge density associated with non-uniform conductivity is of the form:

$$\rho_{tg} = -E(r) \cdot \frac{\varepsilon}{\sigma(r)} \frac{d\sigma(r)}{dr} \tag{2}$$

where ε is the dielectric permittivity of the material. If the temperature dependence of conductivity follows an Arrhenius law with activation energy E_a, the charge density can be written according to the following Equation:

$$\rho_{tg}(r) = -\varepsilon.E(r) \cdot \frac{E_a}{k_B T^2} \frac{dT}{dr} \tag{3}$$

where T is the absolute temperature and k_B is the Boltzmann's constant. It can be noticed from Equations (2) and (3) that space charge polarity depends directly on the conductivity gradient $d\sigma/dr$. For a negative voltage applied to the inner cable conductor, the field $E(r)$ is negative; space charge is negative under a temperature gradient through the insulating material in which electrical conductivity decreases from the inner to the outer conductor of the cable.

Boggs *et al.* (2001) have studied the behavior of resistive field distribution under non-uniform temperature conditions for two types of insulating polymers having different activation energies for the conductivity. Their model demonstrated the importance of using materials having low activation energy (E_a) and large field dependence of conductivity in order to more evenly distribute electric field in conditions of severe thermal gradients.

The field distribution in HVDC cable is controlled by the material conductivity which is strongly varying with temperature and may also vary significantly with electric field. However, the temperature and electric field dependencies of conductivity are specific to each material. Furthermore, space charge accumulation may appear unrelated to temperature gradient within the materials. Thus, electric field distribution may be relatively complex to predict under the presence of temperature gradient and non-homogeneous field conditions.

The objective of this work is to assess the influence of temperature gradient on charge accumulation and electric field distribution in medium voltage cable models (MV-HVDC). These charge/field distributions in the absence and in presence of temperature gradient are estimated by direct measurement or modeled from the temperature and field dependencies of conductivity obtained experimentally. Differences in regard to the behavior are discussed.

2. Experimental Conditions

2.1. Conductivity measurements

Samples used for conductivity measurement consist of plaques of cross-linked polyethylene (XLPE) with thickness varying from 500 to 600µm. Both faces of samples are gold-metalized (50mm diameter electrodes, representing 20cm²

electrodes area). A silicone ribbon was laid at the periphery of electrodes to avoid edge phenomena.

Measurements were performed under different temperatures varying from -10°C to +90°C by step of 10°C. Temperature regulation is achieved through the circulation of thermo-stated fluid inside reservoir used as sample holder. For each of the temperature levels, charging/discharging current measurement were realized for 10 values of applied field ranging between 2 and 25kV/mm under isothermal conditions according to the protocol shown in Figure 1. Polarization/depolarization steps last for 1h/1h. Voltage has been applied by means of a DC generator of 65kV/0.5mA. A new sample has been used for each value of temperature to avoid possible memory effects. Current values were recorded every 2 seconds all along the measurements.

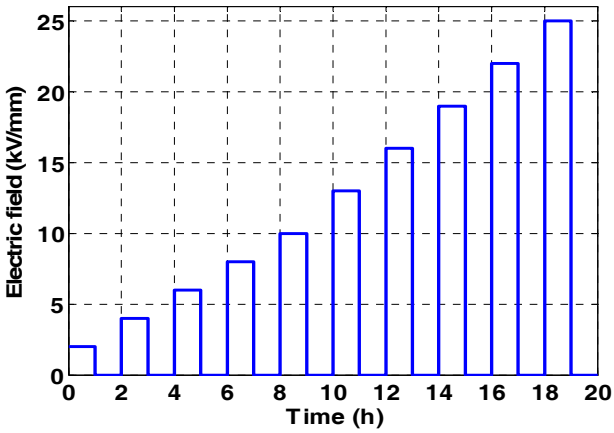

Figure 1. Protocol of conduction current measurement

2.2. Space charge measurements

Tested samples are sections of Medium Voltage cable (MV) XLPE insulation, of about 3 m long and 4.5mm thick insulation. The inner and outer radiuses of insulation are respectively 5 mm and 9.5 mm. The diameter of the inner conductor (made of aluminum) is of 8 mm and the inner and outer Semi-Conductor (SC) thicknesses are respectively 1 and 0.5 mm.

Space charge measurements were carried out using the pulsed-electro-acoustic (PEA) method in the configuration depicted in Figure 2. The PEA cable test equipment was provided by *TechImp,* Italy. The tested cable is fixed on the PEA cell by means of a holder offering the ability of adjusting cable clamping force. This procedure guarantees a good acoustic contact between outer SC of the cable and aluminum electrode of the measuring device.

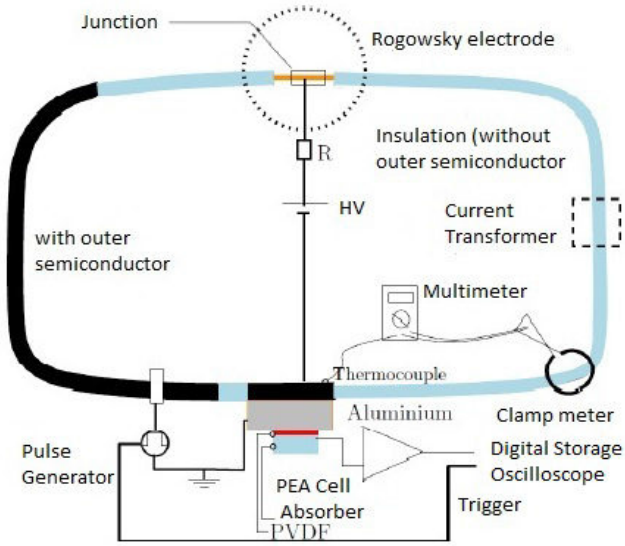

Figure 2. Schematic representation of the PEA Cable system

Pulse voltage, provided by a pulse generator of 5 kV/30ns/10 kHz (of which the frequency is limited to 5 kHz), is injected at the measurement area on the outer SC. To form a decoupling capacitor between the pulse generator and the HVDC generator, the outer SC is removed over a length of 5 cm (cf. Figure 2) between the measurement point and the region where pulses are applied.

High voltage generator supplies DC voltage varying between 0 and -100 kV. The HVDC generator is connected to the inner conductor through a Rogovsky electrode. This type of electrode avoids field intensification which is likely to induce discharges at the connecting areas in the vicinity of the cable and the high voltage source.

In this work, space charge measurements on MV cables were performed under two different thermal conditions: at room temperature and under a temperature gradient of 16°C along the cable radius. For the first condition, cable sample is kept at room temperature whereas for the second, temperatures at the inner and outer semiconductive screens were set to 57°C and 41°C respectively. To achieve such a temperature gradient across the cable insulation, the conductor is heated by a current of 200 A by means of a current transformer, while the external surface of the outer SC is kept in ambient condition. It is further noticed that temperature at the outer surface of the cable in contact with the aluminum shield of the PEA cell is somewhat reduced compared to the surface temperature of section of cables in the air. Thus, we can anticipate that the temperature gradient at the measurement area is higher than somewhere else along the cable suspended in air. We found during

testing that after a period of about 100 minutes of current flow within cable loop, the surface temperature of the cable stabilizes around a value of 41°C. Since the heat flux across the cable radius is constant in steady state condition, the temperature at the inner conductor can be estimated from the temperature measured on the cable surface, the heat generated by Joule effect in the cable conductor and the thermal resistance of cable insulation. We also verified by thermal modeling that the power dissipated in the cable is consistent with the measured temperatures in the room and at the cable surface.

Negative voltage (-40 or -80kV) was applied to the cable conductor during 7 hours for -40kV and 3h for -80kV, followed by 1 hour of depolarization. PEA signals were recorded and averaged every 200 seconds throughout the voltage cycle. Profiles were processed using deconvolution technique to derive space charge density profiles. The deconvolution method used in this work takes into account all phenomena related to acoustic wave generation and propagation in coaxial geometry which consist in attenuation, dispersion, electrostriction and the response of the PEA setup (sensor & voltage pulse) to compute space charge profiles from PEA raw signals. A complete description of the signal processing algorithm is given by Vissouvanadin *et al.* (2014).

3. Results

3.1. Conductivity measurements function of field and temperature

Conduction current measurement results carried out on XLPE material under different conditions of temperature and field are shown in the Figure3 (*J vs. E* characteristics in log-log plot). Data correspond to charging current obtained after 1h of polarization. It must be admitted that a 1h polarization time is not always sufficient to obtain steady state conduction (Vu *et al.*, 2015). It was shown however that the transient nature of the current is not linked to orientation polarization processes. We observe the presence of threshold field separating two different regimes of conduction. Below the threshold, current characteristics exhibit non-linear behavior and the slope of *J vs. E* characteristics is estimated to approximately 1.4 at 20°C. This kind of behavior is likely to appear even in absence of space charge accumulation process provided that carrier mobility is field-dependent. However, space charge is likely to accumulate even at low field for sufficiently high temperature. Above the threshold field, the dependence of current density with field is more pronounced. Conduction current increases rapidly with applied field through a power law $I \propto E^{\alpha}$ with $\alpha >> 1$. Current characteristics exhibit respective slopes of 5.8, 4.1, and 3.7 at 20, 30 and 40°C. Thus conductivity can be expressed in the form of $\sigma(E) \propto E^{\alpha-1}$.

Data from XLPE material have clearly pointed out the strong dependence of conductivity with temperature and electric field. In order to derive an analytical

expression of conductivity with temperature and electric field, the following semi-empirical equation has been used to fit the experimental data:

$$\sigma(T,E) = A.\exp\left(\frac{-E_a}{k_B T}\right).\sinh(B(T).E).E^{\alpha} \tag{4}$$

where A and α are constants. E_a is the activation energy of conductivity. B must be temperature-dependent to take account for the shift in the threshold field with temperature: a linear dependence, $B = a.T + b$, was obtained.

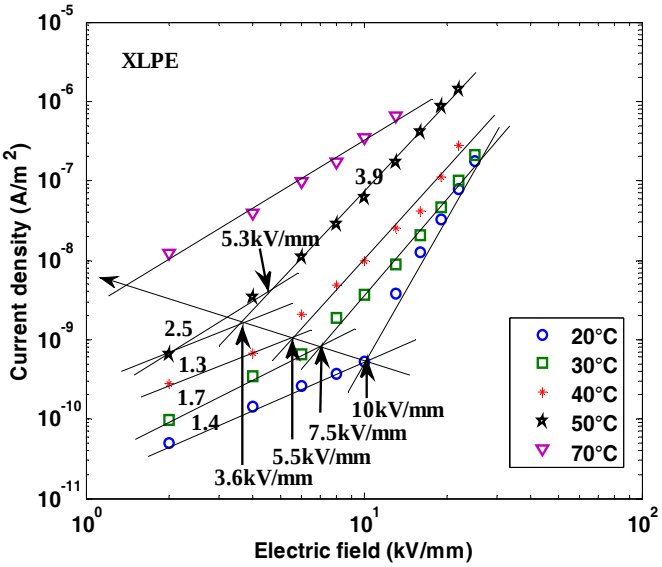

Figure 3. J-E characteristic of XLPE in log-log plot for different temperatures

Note that the model of Eoll (1975) with an exponential dependence of the conductivity as a function of both field and temperature:

$$\sigma(T,E) = \sigma_0.e^{\alpha.T}.e^{k.E} \tag{5}$$

is used in the case of HVDC cables with impregnated paper insulation. There is no theoretical or experimental justification of such law in the case of insulating polymers. Expressions similar to Eq.4 were adopted in the literature for conductivity of synthetic cable insulators (Choo *et al.,* 2011; Boggs *et al.,* 2001; Qin *et al.,* 2012).

Experimental data fits of XLPE for different fields and temperatures have been achieved and model / measurement comparison is presented in Figure 4. It can be argued that there is a fairly good fit between model and data for all field and

temperature values. The coefficients obtained for XLPE in case of Equation (4) are shown in Table 1.

Table 1. Conductivity coefficients derived for XLPE from equation 4. Coefficients given for conductivity in S/m, T in K, field in V/m. k_B =8.62 10^{-5}eV/K

A (SI)	0.8
Ea (eV)	1
B (m/V)	$1.38.10^{-7}$ for T ≤ 313 K
	$-1.3.10^{-9}$ T + $5.45.10^{-7}$ for T ≥ 313 K
α	0.15

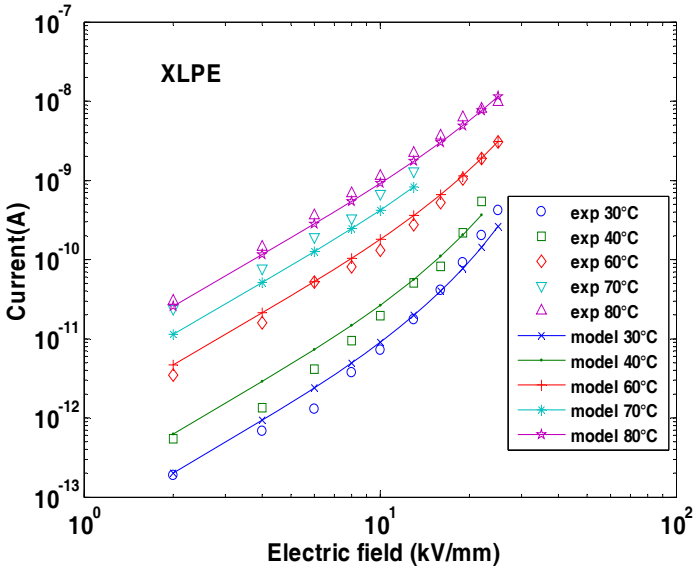

Figure 4. Experimental and fitted current-field characteristics for XLPE at different temperatures

3.2. Simulation results based on the conductivity data

Most of insulating polymers exhibit temperature-dependent conductivity. The field dependence is generally small when considering moderate fields of the order of 1 kV/mm. Design fields considered for synthetic insulation cables are of the order of 15-20kV/mm, and correspond to substantially non-linear regimes if we refer to the data presented above, which are also consistent with data from literature (Bodega *et al.*, 2004; *Delpino et al.*, 2008). Electric field distribution across the cable radius is

thus not easy to derive analytically, even in stationary condition. Such difficulty is overcome by using a numerical solver to compute field distribution in the presence of a temperature gradient. Another advantage of using numerical solution is the ability to obtain solutions under steady state as well as under transient conditions.

The previously established semi-empirical model of XLPE conductivity to take into account changes in temperature and field was introduced into *Comsol Multiphysics®* software for computing field distributions in the MV cables subjected to various electrical and thermal stresses. Negative voltage is applied to the inner conductor and the reference potential is taken on the outer SC.

Figure 5 shows simulation results of electric field profiles along the cable radius, for a polarization time of 7h under -40kV in isothermal condition at room temperature (22°C). The electric field profile does not change substantially with polarization time and its distribution is similar to that of the Laplacian field (corresponding to the distribution at time=0s). The electric field module decreases and increases respectively at the internal and external conductor. This phenomenon comes from the fact that field at the internal SC is higher at the beginning of polarization (capacitive distribution), which implies a higher conductivity. Steady state is reached when the total current, i.e. the quantity $\sigma(r).E(r).r$ is constant over the radius r (cf. Equation (1)). Consequently, field as well as conductivity decrease at the vicinity of the internal SC. Conversely, at the outer electrode, since insulator conductivity is initially low (the initial field being lower), field magnitude increases with time. After 7 hours of polarization, electric field values were estimated by the model to 11.8kV/mm and 6.8kV/mm at the inner and outer semiconductors, respectively.

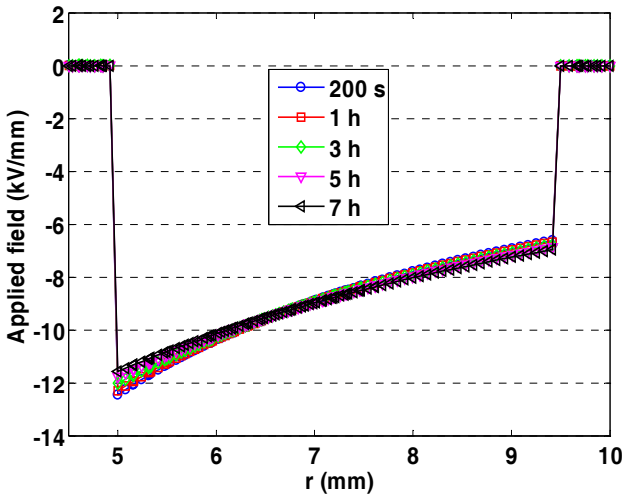

Figure 5. Electric field profiles calculated for MV cable at different times under -40 kV at room temperature

In addition, charge accumulation of the same polarity (not shown on the profiles) as the applied voltage (negative in this case) is associated to this evolution of electric field. In these conditions, space charge density is relatively low. The maximum density near the inner semiconductor is about -10 mC/m^3 after 7 h of polarization.

For a thermal gradient of 16°C (41 and 57°C at the outer and inner semiconductors, respectively), we obtained space charge density and electric field profiles shown in Figure 6 for an applied voltage of -40 kV.

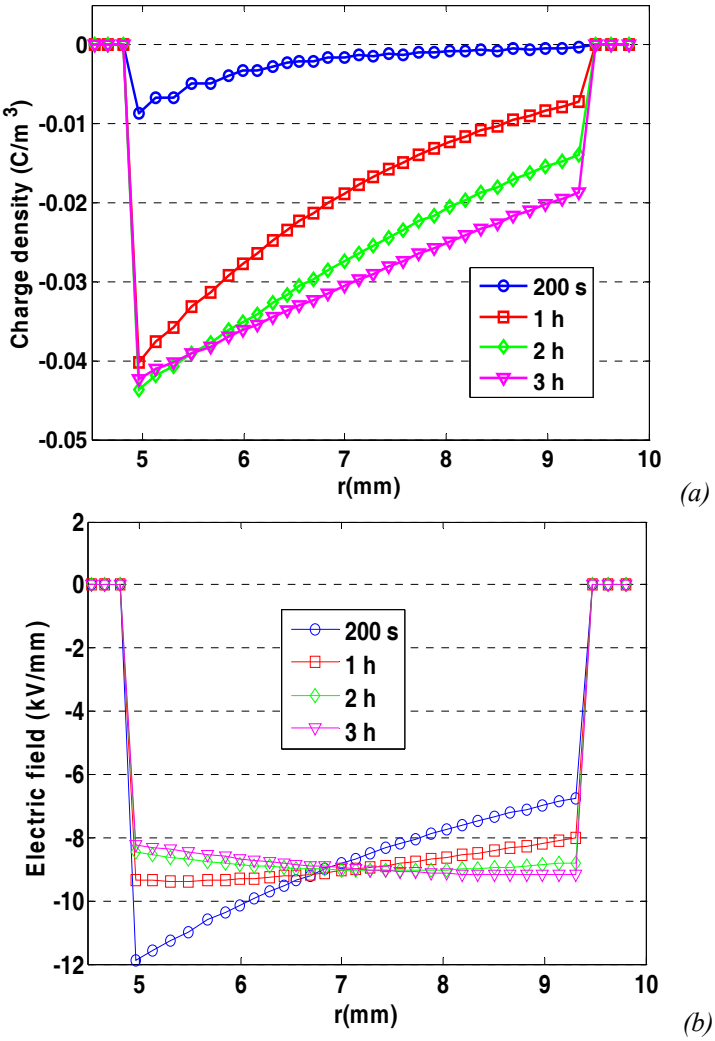

Figure 6. Space charge (a) and electric field (b) profiles calculated for the MV cable to different time under -40 kV and thermal gradient of 16°C

According to Figure 6a, negative charges accumulate rapidly adjacent to the inner electrode during the first hour of polarization. After 2h, charge density ranges from -43mC/m^3 to -14mC/m^3 along the cable radius. Thereafter, charge density decreases slightly adjacent to the inner electrode and increases continuously at the outer electrode and reaches values of -42mC/m^3 and -19mC/m^3 at the inner and outer semiconductor, respectively, after 3h of polarization. As a result, the electric field decreases and increases respectively with time at the inner and outer electrode (Figure 6b). The maximum field is located in the middle of the insulator after 2h of polarization and stress profile is reversed (compared to the Laplacian field) after about 3 hours of polarization. A maximum field of about 9kV/mm is obtained at the external electrode after 3h of polarization. Moreover, we note that field magnitude remains almost invariant in the middle of cable insulation.

To be in agreement with the applied electric field conditions during measurements (cf. § 3.3), the stress cycle in the model was supplemented by 1 h of depolarization (short circuit), followed by 3 hours of polarization under -80kV. Figure 7 shows the modeled space charge and field distributions as a function of time under -80kV. After 200s of polarization, the field deviates significantly from the Laplacian field and is quickly reversed, roughly after 1h of polarization. This phenomenon is in part due to the fact that the charges accumulated in the previous polarization step (under -40kV) were not relaxed during the short circuit step and thus give rise to a residual field. Moreover, a large accumulation of negative charges is predicted in the all insulation, with a strengthening towards the inner SC when voltage is increased to -80kV. The point of maximum field shifts from the internal electrode to the external electrode (stress reversal phenomenon) after 1 hour of polarization. The field distribution becomes stationary with values of 17kV/mm and 18.5kV/mm at the inner and outer SC respectively.

3.3. Space charge measurement results

In the following, the evolution of space charge profiles and electric field in the cable insulation predicted according to the above model are compared to experimental measurements of space charge carried out on cables under different conditions of temperature and voltage.

Figure 8 shows charge density profiles and electric field distributions in the cable insulation under -40 kV at room temperature for different polarization times. In Figure 8a, it is observed that, immediately after voltage application, positive charges are accumulated in the bulk, slightly towards the outer semiconductor, whereas negative charges build up adjacent to this electrode. The density of positive and negative charges increases with polarization time and reaches steady values after 5h of polarization. However, positive and negative charge densities are relatively low, of the order of 80mC/m^3 and 40mC/m^3, respectively.

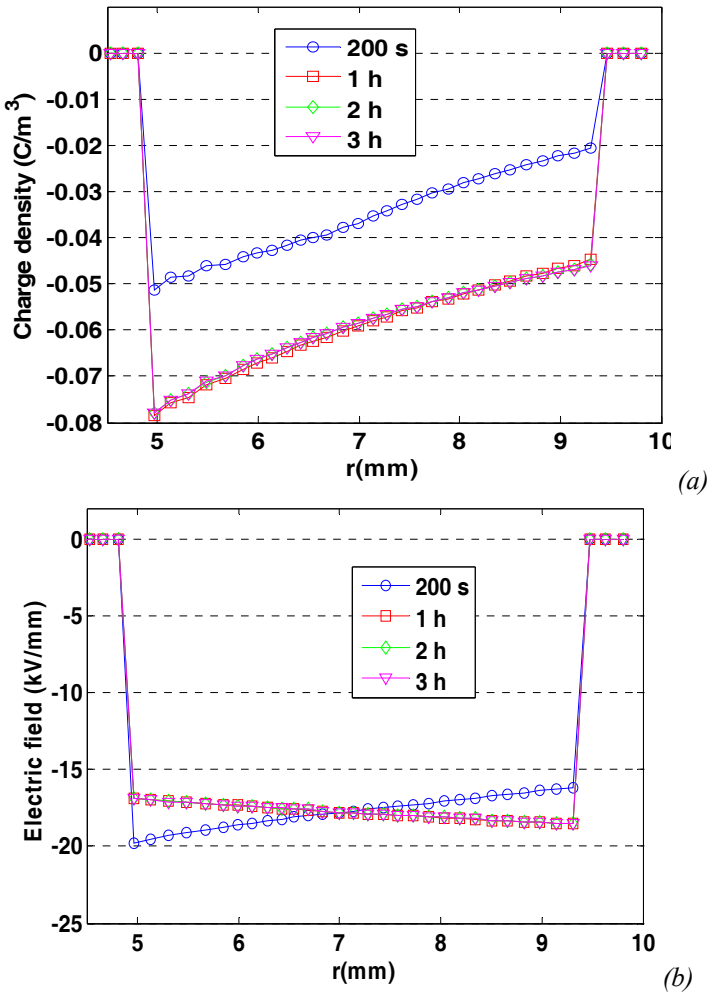

Figure 7. Electric field profiles calculated for the MV cable to different time under -80 kV and thermal gradient of 16°C

The field distribution in the insulation under -40 kV is shown in Figure 8b. The maximum field remains at the inner SC throughout the polarization procedure. Field profiles are not deviating much from the Laplacian field distribution due to the low charges accumulation. For instance, under -40kV, at short time following the voltage application, field magnitudes are approximately 12.8kV/mm and 4kV/mm at the internal and external SC, respectively. After 7h of polarization, the field magnitudes are in the order of 13kV/mm and 2kV/mm at the internal and external SC respectively. These values do not deviate significantly from the Laplacian field (12kV/mm and 6kV/mm at inner and outer SC for a capacitive distribution).

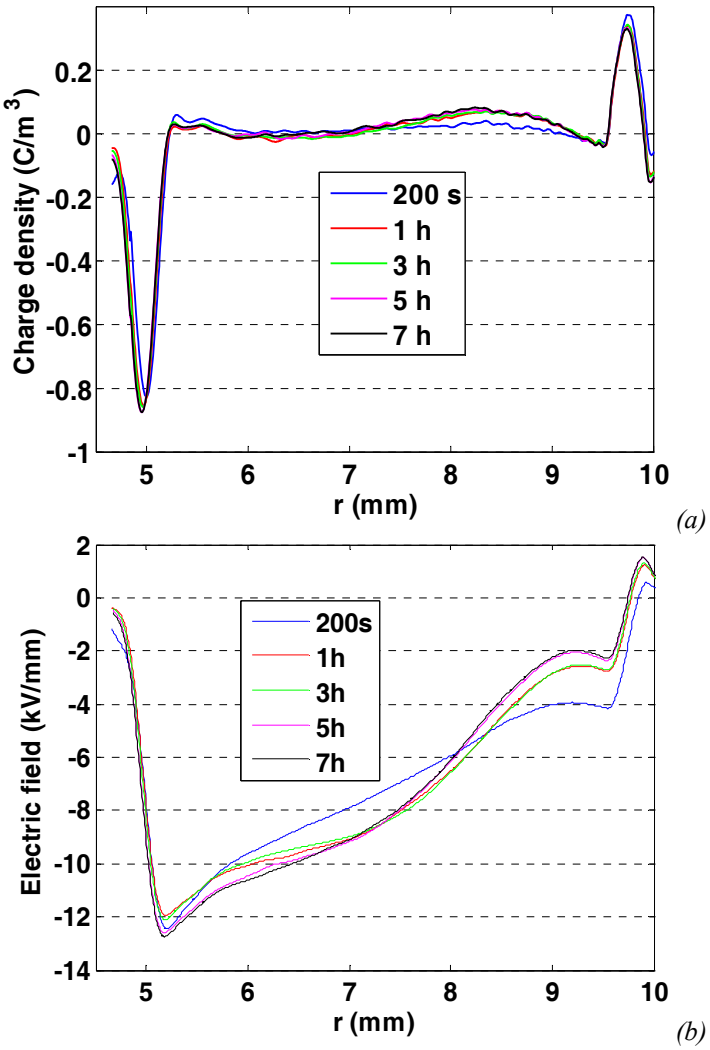

Figure 8. Space charge (a) and electric field (b) profiles measured for the MV cable at different times under -40 kV at room temperature

Figure 9 shows the color-scaled spatio-temporal space charge density pattern as a function of cable radius for applied voltages of -40kV and -80kV measured under a temperature gradient of 16°C. In this representation, the X axis corresponds to polarization time while Y axis corresponds to the position in the cable insulation (radius). Blue and red colors correspond to negative and positive charges, respectively. During the polarization step under -40 kV, negative charges are injected at the inner SC (*i.e.* at r=5 mm in Figure 9) and tend to move in time

towards the outer SC. Positive charges are also visible next to the outer SC. The density of negative charges in the bulk of the insulation is relatively low, of the order of 70 mC/m^3 after 3 h of polarization. During the depolarization step following the polarization at -40 kV, the evolution of charge distribution is relatively slow indicating that positive and negative charges are deeply trapped in the material.

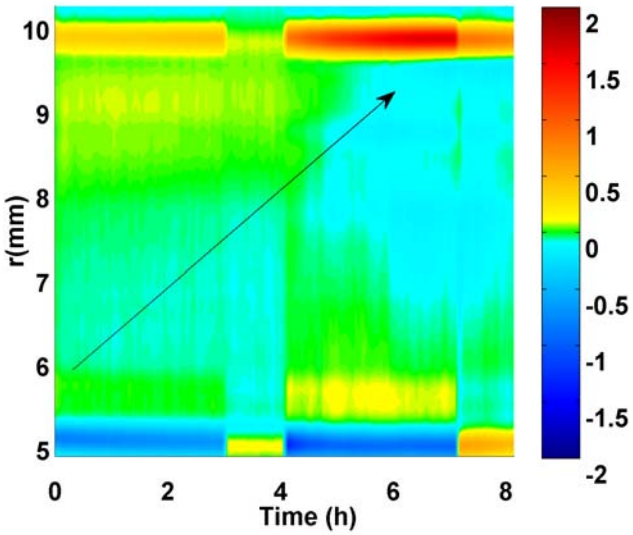

Figure 9. Cartography of space charge density in a model cable under -40 kV and -80 kV in the presence of a thermal gradient of 16°C. The color bar represents the scale for charge density in C/m³

The beginning of the polarization step at -80kV is clearly marked by negative charges transiting from the cathode to the anode. Negative charges reach the outer conductor after about 5 h forming heterocharges. The maximum density of negative charges is of the order of 0.2C/m^3 at the end of the polarization step at -80 V.

Electric field distributions obtained at different times under the two applied voltage levels are shown in Figure 10. Under -40 kV (Figure 10a), field decreases with time at the inner SC and increases in the bulk at the vicinity of the outer SC during 3 hours of polarization. The maximum field moves from the inner conductor to the center of the insulator after 1 h of polarization due to the accumulation of negative charges in the bulk. The point of maximum stress tends to move over time towards the outer electrode similarly to that of negative charges.

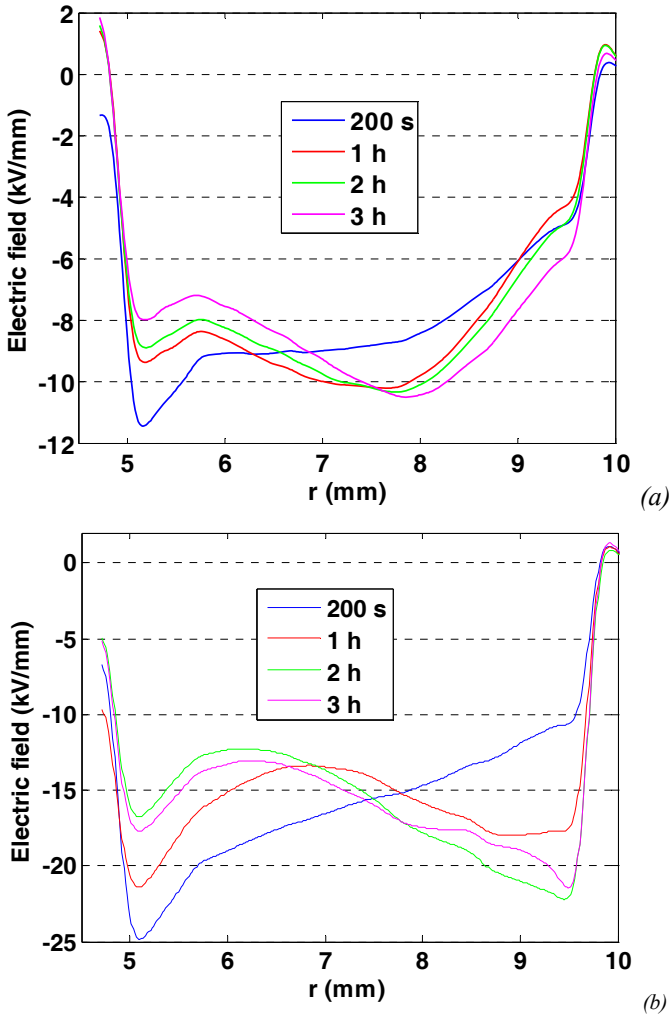

Figure 10. Electric field profiles measured for the MV cable at different times under -40kV (a) and -80 kV (b), with a temperature gradient of 16°C.

Under -80kV, the position of the maximum stress is switching from the inner electrode to the outer electrode after 2h of polarization (6 hours of measurement). This shift in position is due to the arrival of negative charges at the outer SC where they form heterocharges. At the end of the polarization step, field modules at the inner and outer SC are estimated to about 16.5kV/mm and 22kV/mm, respectively.

From the results in the absence and in the presence of temperature gradient, it is noted that the densities of charges accumulated at room temperature are lower

compared to those measured in the presence of temperature gradient due essentially to the non-homogeneous electrical conductivity across the cable insulation.

At room temperature, electric field distortions in the insulation for both values of applied voltage (-40kV and -80kV) are considered as relatively low and field profiles are close to the Laplacian field. The positions of maximum and minimum fields remain at the internal and external SC, respectively. Transient processes and deviations from the Laplace distribution field are solely due to the nonlinear nature of conductivity versus electric field. Conductivity variations with field remain moderate compared to those observed with temperature.

4. Discussion

In insulating polymers, especially out of the low field limit (beyond some kV/mm), the concept of conductivity in the sense of intrinsic carriers transport is probably not much more than an empirical way of handling the dielectric response: using bipolar transport models, space charge and current in insulating polymers could be fully described considering processes as injection, transport, trapping and recombination of charges (Boufayed *et al.,* 2006). Such models probably provide a more realistic description of phenomena at play than does the approach through 'conductivity' but are quite demanding in terms of experimental data and hypotheses to verify to parameterize the processes. In connection to this, one could wonder if space charge measurements can actually probe mobile charges involved in conduction as they do necessarily couple to the material. First, in insulating polymers, it is generally agreed that there is no conduction through band states, but to shallow states formed by disorder associated to materials (Teyssedre, Laurent, 2005). So, apparent mobilities for 'mobile' charges remain low, being less than 10^{-12}m²/V/s, and all charges spend most of the time on traps and can efficiently couple to the material. Second, the case of mobile charges and related screening effects in space charge measurements in semiconductor devices has been addressed by Holé *et al.* (2002, 2004). Both mobile and trapped charges appear in principle measurable and derivation of the method has been given for pressure pulse excitation.

Comparing electric field (and charges) profiles obtained by simulation and measurement, a number of differences can be identified, such as the presence of positive charges in measurement, not predicted by the model, or the fact that field values or the kinetics of field variations are different. Let's consider first how different are measurement conditions, on one hand, and assumptions on physical phenomena, on the other hand.

– Modeling is based on conductivity measurements on XLPE, carried out on plaque samples with gold electrodes. These conditions are actually not representative of cables, since the cross-linking conditions of samples, the degree of degassing and the nature of electrodes are likely to be different. Thus ion generation, or charge injection mechanisms may not occur in the same conditions.

– In simulation, charge accumulation is considered only as a result of non-uniform conductivity due to the divergence of field and temperature gradient. Conductivity gradient could be present due to insulation properties gradient along the radius (associated to cable extrusion conditions), a feature which is not hypothesized therein.

– According to the copious amount of space charge data available for XLPE in plaque geometry, it is well known that charges accumulation is not only due to the temperature and electric field dependencies of conductivity; other processes related to the formation and movement of ionic species or to conduction mechanisms controlled by the presence of space charge may also take place. It is therefore interesting to compare field distributions obtained from the model with the restrictive assumption of macroscopic transport scheme, to space charge measurements, to determine, for example, whether the effects of thermal gradient are dominant on electric field distribution.

In the absence of thermal gradient, charges accumulation under an applied voltage of -40kV is slow and weak, whichever measurement or simulation results are considered. Accordingly, the electric field distribution does not substantially deviate from Laplacian field. However, it may be noted that the density and nature of charges obtained in simulation and in experiments are different; charge densities obtained experimentally being higher than in simulation. This difference indicates that other charges generation mechanisms such as injection or impurities dissociation are operative and even predominate over processes related to conductivity gradient. These mechanisms, however, remain difficult to identify by considering solely space charge profiles presented in Figure8a. The use of polarity inversion could be a way to discriminate space charge processes purely related to the conduction gradient from those induced by charge trapping and ionic processes: whereas conduction processes should lead to completely symmetrical response (i.e. change of sign of the charge and field all along the profile), processes related to transport and ionic contributions should provide space charge patterns that depend on the actual properties of the carriers involved like mobility. However, the used set-up is equipped with negative voltage source only at the time current experiments are realized.

In the presence of temperature gradient, simulation and measurement results exhibit same charge polarity. Negative charges appear in the bulk of the insulation. However, charges distribution according to the model is more uniform than that obtained in experiments. For simulation, the average density of charges in the insulation is respectively about 30mC/m^3 and 60mC/m^3 under -40kV and -80kV; charges build-up first in the region adjacent to the inner screen as a consequence of the shorter time constant (ε/σ). Measured charge densities adjacent to the outer electrode are respectively 70mC/m^3 and 200mC/m^3 under -40and -80kV, after 3h of polarization. This leads to a considerable difference regarding electric field distribution between simulation and measurement. For simulation, field increases monotonously from the inner electrode towards the outer electrode after 3 h and 1 h

of polarization, under -40kV and -80kV respectively (i.e. stress inversion phenomenon occurs). Moreover, measurement results show that the minimum field value appears in the bulk of the insulation close to the inner conductor for both voltages. The nature of the electrodes is a possible reason of these differences. Charges are computed by simulation under the assumption of perfect ohmic contacts (charges are freely injected into or extracted out the insulator). The heterocharges observed experimentally may be due to a possible presence of a potential barrier for charges extraction at the external SC. Another possibility is positive charge build-up adjacent to the cathode due to the accumulation of ionic species. Crosslinking residues are indeed known to favor the heterocharges formation (Sekii *et al.*, 2009; Lan *et al.*, 2014). Nevertheless, a fairly good estimate of the steady state electric field distribution can be obtained from simulation based on space charges induced-conductivity gradient.

5. Conclusions

Based on experimental results on conduction current in cross-linked polyethylene samples in film shape, a semi-empirical expression of conductivity function of temperature and electric field is proposed. This analytical model is used to predict the space charge and field distributions in the absence and presence of temperature gradient in a medium-voltage cable.

Experimental space charge measurements were obtained on XLPE-insulated MV cables by using the pulsed electroacoustic method applying a negative potential to the cable conductor, either in isothermal conditions or under temperature gradient. In presence of a temperature gradient, the build-up of negative charges in the insulation and the formation of heterocharges at the outer SC are observed. As a result, the field distribution is distorted and reversed with regard to the Laplacian field. Experimental results are broadly in line with the model. However, the model predicts a continuously decreasing density of negative charges when going from inner to outer SC. The heterocharge formation due to transport of ionic moieties is one of the probable reasons for the differences. *In fine*, measured field distortions tend to be higher than predicted. Measurements remain therefore a necessary step in the control of field distribution in HVDC cables.

Bibliography

Bodega R., Montanari, G.C., Morshuis P.H.F. (2004). Conduction current measurements on XLPE and EPR insulation, *2004 Annual Rep. IEEE Conf. Electr. Insul. Dielectr. Phenom. (CEIDP)*, p. 101-105.

Boggs S., Dwight H., Hjerrild J., Holbol J.T., Henriksen M. (2001). Effect of insulation properties on the field grading of solid dielectric DC cable. *IEEE Trans. Power Deliv.*, vol. 16, n° 4, p. 456-462.

Boufayed F., Teyssèdre G., Laurent C., Le Roy S., Dissado L.A., Ségur P., Montanari G.C. (2006). Models of bipolar charge transport in Polyethylene. *J Appl. Phys.* vol. 100, p. 104-105.

Choo W., Chen G., Swingler S.G. (2011). Electric field in polymeric cable due to space charge accumulation under DC and temperature gradient. *IEEE Electr. Insul. Mag.*, vol. 25, n° 3, p. 596-606.

Delpino S., Fabiani D., Montanari G.C., Laurent C., Teyssedre G., Morshuis P.H.F., Bodega R., Dissado L.A. (2008). Polymeric HVDC cable design and space charge accumulation. Part 2: Insulation interfaces. *IEEE Electr. Insul. Mag.*, vol. 24, n° 1, p. 14-24.

Eoll C.K. (1975). Theory of stress distribution in insulation of High-Voltage DC cables: Part I. *IEEE Trans. Electr. Insul.*, vol. 10, n° 1, p. 27-35.

Fabiani D., Montanari G.C., Laurent C., Teyssedre G., Morshuis P.H.F., Bodega R., Dissado L.A. (2008). HVDC cable design and space charge accumulation. Part 3: Effect of temperature gradient. *IEEE Electr. Insul. Mag.*, vol. 24, n° 2, p. 5-14.

Holé S., Ditchi T., Lewiner, J. (2002). Can non-destructive space charge measurement techniques have fallout in other fields? *Proc. 11th Internat. Symp. Electrets (ISE)*, p. 32-35.

Holé S., Lewiner, J. (2004). Direct measurement of trapped and free charge distributions in semiconductors. *Appl. Phys. Lett.* vol. 84, p. 1308-1310

Lan L., Wu J., Yin Y., Zhong Q. (2014). Investigation on heterocharge accumulation in crosslinked polyethylene: Experiment and simulation. *Jpn. J. Appl. Phys.*, vol. 53, n° 7 (071702).

McAllister I.W., Crichton G.C., Pedersen A. (1994). Charge accumulation in DC cables: A macroscopic approach. *Proc. IEEE Internat. Symp. Electr. Insul. (ISEI)*, p. 212-216.

Mazzanti G., Marzinotto M. (2013). *Extruded Cables for High-Voltage Direct-Current Transmission*, Wiley-IEEE Press. New Jersey.

Qin Shanshan, Boggs S. (2012). Design considerations for High Voltage DC components. *IEEE Electr. Insul. Mag.*, vol. 28, n° 6, p. 36-44.

Sekii Y., Maeno T. (2009). Generation and dissipation of negative heterocharges in XLPE and EPR. *IEEE Trans. Dielectr. Electr. Insul.*, vol.16, n° 3, p.668-675.

Teyssedre G., Laurent C. (2005). Charge Transport Modeling in Insulating Polymers: From Molecular to Macroscopic Scale. *IEEE Trans. Dielectr. Electr. Insul*., vol. 12, p. 857-875

Vissouvanadin B., Vu T.T.N., Berquez L., Le Roy S., Teyssedre G., Laurent C. (2014). Deconvolution techniques for space charge recovery using pulsed electroacoustic method in coaxial geometry. *IEEE Trans. Dielectr. Electr. Insul.*, vol. 21, n° 2, p. 821-828.

Vu T.T.N., Teyssedre G., Vissouvanadin B., Le Roy S., Laurent C. (2015). Correlating conductivity and space charge measurements in multi-dielectrics under various electrical and thermal stresses. *IEEE Trans. Dielectr. Electr. Insul.*, vol. 22, p. 117-127.

Receveid: 27 February 2015
Accepted: 29 October 2015